MACROSCOPIC MODELING OF R.F. PLASMA DISCHARGES

by

G. R. Misium, A. J. Lichtenberg, and M. A. Lieberman

MACROSCOPIC MODELING OF R.F. PLASMA DISCHARGES

by

G. R. Misium, A. J. Lichtenberg, and M. A. Lieberman

ELECTRONICS RESEARCH LABORATORY

College of Engineering
University of California, Berkeley
94720

MACROSCOPIC MODELING OF R.F. PLASMA DISCHARGES

by

G. R. Misium, A. J. Lichtenberg, and M. A. Lieberman

ELECTRONICS RESEARCH LABORATORY

College of Engineering
University of California, Berkeley
94720

Macroscopic Modeling of R.F. Plasma Discharges

by

G.R. Misium, A.J. Lichtenberg, and M.A. Lieberman

Department of Electrical Engineering and Computer Sciences

and the Electronics Research Laboratory

University of California, Berkeley, CA 94720

ABSTRACT

We describe a self-consistent model of a symmetric plane parallel r.f. discharge. The model is built upon basic laws such as conservation of particles and energy, and is capable of predicting rapidly the important discharge parameters from a processing point of view, such as the ion energy and flux to the electrodes. ·The following physics is incorporated into the model: energy dependent electron-neutral ionization, excitation and elastic scattering; nonuniform, self-consistent collisionless and collisional r.f. sheaths; electron ohmic heating by elastic scattering in the sheaths and bulk plasma and stochastic heating by the oscillating fields in the sheaths; electron energy losses to neutrals through collisions and to the electrodes; ambipolar ion diffusion; and total r.f. power balance. A set of equations describing this dynamics has been obtained and used in a code to simulate different discharges. The model has proven to be useful in comparing the effect of varying parameters on the discharge. Comparisons with experimental results show a good agreement between predicted and measured parameters.

I. INTRODUCTION

Capacitive r.f. plasma discharges are extensively used in the semiconductor industry for etching and sputtering processes, and their use has become critical for VLSI production. Although many phenomena occurring in these discharges have been studied during the last years[1-13], there is no self-consistent model capable of predicting rapidly the plasma state of a discharge given a set of independently controllable parameters. Monte Carlo simulations of r.f. discharges have been performed[14-15], although self-consistent solutions have not been obtained. Particle[16-17] and fluid[18-22] simulations have been applied to treat various idealized models in certain parameter regimes. These numerical simulations, while promising, are costly in computer time, such that only a few solutions for specific chosen parameters have been obtained. Consequently, it has not been possible to do parametric studies using these approaches.

In this work, we describe a self-consistent macroscopic model that is capable of predicting the main discharge parameters from a processing point of view, such as the ion energy and ion flux to the electrodes. The model is formulated in terms of separate physical descriptions of the sheath and the "glow" or bulk plasma regions of the discharge, which are then coupled at the boundaries. This approach, pioneered by Godyak and his collaborators[3-9], not only describes the basic dynamics of the discharge, but can be used as a tool to predict the correlations among the different parameters of the discharge, to design new processes, and to simulate the topography of etching processes. By its very nature, computation is used only to present numerical values of the analytical solutions, and is therefore very efficient in computer time.

The model is developed for a symmetric plane parallel discharge that is symmetrically driven by an r.f. power source, as shown in Fig. 1. The plasma is created between two electrodes of area A separated by a distance l. The discharge is considered to be composed of a bulk plasma region of thickness l_p separated from the electrodes by two sheaths, each having time-average thickness s_0. The discharge is driven by an r.f. supply at a frequency ω for which the electrons respond rapidly to the r.f. electric field, while the ions respond only to the d.c. field. The model incorporates realistic physical assumptions for electron heating, electron impact on neutral gas atoms, and electron and ion transport.

Electron processes include: energy dependent ionization, excitation, and elastic scattering; electron energy losses to the electrodes; electron ohmic heating in the sheaths and bulk plasma; stochastic heating by the oscillating fields in the sheaths; secondary electron emission; and secondary electron-neutral ionization. Ion processes include ion energy losses to the electrodes; ambipolar ion diffusion; ion acceleration in self-consistent sheaths; and production of secondary electrons.

In Sec. II, we develop the basic model describing the discharge using the equations for particle and energy balance within the glow and sheath regions and the continuity of current flow in the discharge. A computer code is used to solve the model equations[23]. Given the discharge length l, pressure p, r.m.s. voltage V_{rf}, frequency ω, and secondary emission coefficient γ, the code determines the electron temperature T_e, density n, r.m.s. current density J_{rf}, r.f. power P_{rf}, ion current density J_i to the electrodes, d.c. sheath self-bias voltage V_s, and the effective discharge circuit parameters. In Sec. III, some code results are presented and comparisons are given to measurements performed in our laboratory and to other published experimental results.

II. BASIC MODEL

We summarize the assumptions used to develop the model:

(1)   The discharge is symmetric and one-dimensional.

(2)   The discharge is divided into two regions, the sheaths and the bulk plasma.

(3).   Electrons have an isotropic Maxwellian distribution of velocities.

(4)   Electrons gain energy through ohmic heating in the bulk plasma and stochastic heating by the oscillating sheaths.

(5)   Thermal electrons lose energy by collisions with neutrals and by escaping to the electrodes.

(6)   Collisional processes in the sheaths include ion charge transfer, ohmic heating, and secondary electron ionization.

(7)   Ions enter the sheaths with the Bohm velocity.

(8)   The ions are cold.

(9) Ambipolar diffusion is the dominant mechanism for ion diffusion in the plasma region at the higher pressures.

(10) Free fall (collisionless, inertia-limited) flow dominates the ion loss from the plasma at the lowest pressures.

(11) Neutrals are ionized through collisions with the bulk plasma electrons and secondary electrons generated at the electrodes.

(12) Secondary electron dynamics are described using a constant velocity transport model.

(13) The electron-neutral collision rates are described by the experimental, energy dependent cross sections for the corresponding collision phenomena.

Using the preceding assumptions, the basic equations for the model are now derived.

Secondary electrons — Secondary electrons can play a significant role in ion production and loss within the discharge. The continuity equation for secondary electrons in the mean free path regime short compared to the device size is

$$\frac{\partial n_{se}}{\partial t} + \frac{\partial \Gamma_{se}}{\partial z} = -\frac{n_{se}}{\tau_c} \, , \tag{1}$$

where n_{se} is the density, Γ_{se} is the flux, and τ_c is the collisional lifetime of the secondary electrons. Since there are two electrodes, we decompose $\Gamma_{se} = u_{se}(n_{se}^+ - n_{se}^-)$ and $n_{se} = n_{se}^+ + n_{se}^-$, where u_{se} is a constant secondary electron velocity. If we assume that $n_{se}^+(z) = n_{se}^-(l - z)$ and that the secondary electrons move with a constant velocity, then we can obtain the following steady state expression for the secondary electron density:

$$n_{se} = n_{se0} \frac{\cosh \left[(\tfrac{1}{2}l - z)/\lambda_{se} \right]}{\cosh (\tfrac{1}{2}l/\lambda_{se})} \, , \tag{2}$$

where n_{se0} is the density of the secondary electrons at the electrode $z = 0$, and $\lambda_{se} = \tau_c u_{se}$ is the mean free path. By integrating (2) and assuming that at the electrode surface

$$\Gamma_{se}(0) = -\Gamma_{se}(l) = -\gamma \Gamma_i(0) \, ,$$

where $\Gamma_i(0)$ is the ion flux incident on the electrode, we determine n_{se0} as

-4-

$$n_{se0} = -\frac{\gamma\Gamma_i(0)\tau_c}{\lambda_{se}} \coth\left(\tfrac{1}{2}l/\lambda_{se}\right) . \tag{3}$$

For long collisional mean free paths we must modify (2) and (3) to account for the escape of secondary electrons to the walls. To do this, we keep the form (2) for the electron density but modify τ_c in (1) as

$$\tau_c^{-1} \rightarrow \tau_l^{-1} = \tau_c^{-1} + \tau_{rf}^{-1} , \tag{4}$$

where τ_{rf} is the collisionless secondary electron loss time to the sheaths. This yields an effective mean free path

$$\lambda_{se} = \tau_l u_{se} \tag{5}$$

that is used in (2) and (3).

The collision loss time τ_c can be written as the time between secondary electron neutral ionizing collisions, times the number of these collisions in which secondary electrons with average energy eV_s may participate; that is,

$$\tau_c = \frac{1}{\nu_{is}} \frac{eV_s}{\mathcal{E}_c} , \tag{6}$$

where ν_{is} is the secondary electron ionization frequency, V_s is the d.c. self-bias voltage across the sheath, and $\mathcal{E}_c$ is the energy lost per ionization.

A secondary electron can escape from the plasma before being thermalized through collisions with neutrals. The discharges that we are modeling are such that the transit time across the plasma for a secondary electron is much smaller than the r.f. period. Consequently, the time a collisionless electron is trapped in the system depends on the potential barriers it finds at the sheaths. For instance, an electron will escape after crossing the plasma once if it is injected into the system when the voltage across the sheath is larger than that across the opposite sheath. Likewise, if the electron is reflected after a first pass through the plasma, it will escape to the same electrode where it was injected if the voltage across the sheath is smaller than when the electron was born. Considering this collisionless dynamics and averaging over all phases of the r.f. voltage, we obtain the mean value

$$\tau_{rf} = T/2\pi , \tag{7}$$

where $T = 2\pi/\omega$ is the r.f. period.

An important effect that has not been incorporated into the model is electron multiplication in the sheath[4]. This limits the validity of our model to the regime for which $\lambda_{se} \gg s_0$, which corresponds to pressures $p \leq 100$ mTorr.

Ion continuity — We assume that the ion and thermal electron transport in the bulk plasma is by ambipolar diffusion and that the relative density and net flux of secondary electrons is small, such that

$$\Gamma = -D_a \frac{dn}{dz} , \tag{8}$$

where Γ is the thermal particle flux and D_a is a constant ambipolar diffusion coefficient. The continuity equation in the steady state is

$$\frac{\partial \Gamma}{\partial z} = \nu_{iz} n + \nu_{is} n_{se} , \tag{9}$$

where ν_{iz} is the thermal electron-neutral ionization frequency. Although n_{se} is generally very small, secondary electrons can be an important source term in the continuity equation because of their high ionizing efficiency. Substituting (3) and (8) into (9), we obtain

$$-D_a \frac{d^2 n}{dz^2} = \nu_{iz} n - \frac{\gamma \Gamma_i(0)\tau_i \nu_{is}}{\lambda_{se} \sinh(\frac{1}{2}l/\lambda_{se})} \cosh[(\tfrac{1}{2}l - z)/\lambda_{se}] ,$$

which has the solution

$$n = A \cos[\kappa(\tfrac{1}{2}l - z)] - B \cosh[(\tfrac{1}{2}l - z)/\lambda_{se}] , \tag{10}$$

where

$$B = -\frac{\gamma \Gamma_i(0)\tau_i \nu_{is}}{\lambda_{se}(\nu_{iz} + D_a/\lambda_{se}^2)\sinh(\frac{1}{2}l/\lambda_{se})} = -\bar{B}\Gamma_i(0) \tag{11}$$

and $\kappa = (\nu_{iz}/D_a)^{1/2}$. Letting $n(l/2) = n_0$ in (10), we solve to obtain $A = n_0 + B$. We then insert (10) into (8), obtaining

$$\Gamma = -(n_0 + B)\kappa D_a \sin[\kappa(\tfrac{1}{2}l - z)] - B(D_a/\lambda_{se})\sinh[(\tfrac{1}{2}l - z)/\lambda_{se}] . \tag{12}$$

We assume that ions leave the plasma at the ion sheath edge $z = s_0$ with the Bohm speed u_B, such that

$$\Gamma(s_0) = -n(s_0)u_B , \tag{13}$$

where

$$u_B = (kT_e/M)^{1/2} . \tag{14}$$

Inserting (10) into (13) and equating to (12), we obtain the ion continuity equation:

$$u_B \left[1 - \Lambda_{se} \frac{\cosh(\frac{1}{2}l_p/\lambda_{se})}{\cos\theta} \right] = \kappa D_a \tan\theta + \Lambda_{se} \frac{D_a}{\lambda_{se}} \frac{\sinh(\frac{1}{2}l_p/\lambda_{se})}{\cos\theta} , \tag{15}$$

where $\Lambda_{se} = B/(n_0+B)$ is a coefficient that accounts for the effect of the secondary electrons and where $\theta = \kappa l_p/2$. We note that $\cos\theta$ is the ratio of the density at the plasma-sheath edge to that at the center of the discharge.

To determine Λ_{se}, we assume that the only ionization mechanism within the sheath is due to secondary electrons. Then writing $d\Gamma/dz = n_{se}\nu_{se}$ within the sheath, we integrate using (2) to obtain

$$\Gamma(0) = \Gamma(s_0) + \frac{\nu_{is}\gamma\Gamma(0)\tau_l}{\sinh(\frac{1}{2}l/\lambda_{se})} [\sinh(\frac{1}{2}l/\lambda_{se}) - \sinh(\frac{1}{2}l_p/\lambda_{se})] . \tag{16}$$

Then using (11), evaluating (12) at s_0, and substituting into (16), we obtain

$$\Lambda_{se} = \frac{\kappa D_a \sin\theta}{\lambda_{se}\nu_{is}\sinh(\frac{1}{2}l_p/\lambda_{se}) - [\lambda_{se}\nu_{is}+D_a/\lambda_{se}][1-(\gamma\tau_l\nu_{is})^{-1}]\sinh(\frac{1}{2}l/\lambda_{se})} . \tag{17}$$

In the limit that secondary electrons are not important ($\gamma \rightarrow 0$), we obtain $\Lambda_{se} \rightarrow 0$ and

$$u_B = \kappa D_a \tan\theta . \tag{18}$$

For completeness, we can consider the limiting case of a uniform density distribution, which is obtained for $D_a \rightarrow \infty$ (a non-physical assumption). For this case, we also find $\Lambda_{se} \rightarrow 0$, and we obtain from (18) the simplest form for the ion continuity equation; that is,

$$u_B = \nu_{is} l_p/2 . \tag{19}$$

The ambipolar diffusion coefficient is usually written as[24] $D_a = D_{a0}/p$, where p is the gas pressure, with typical values of D_{a0} of 5000-15000 cm^2-Torr/sec. However, in a discharge in which the ion

transport is dominated by resonant charge transfer of ions against parent neutral gas atoms, the charge transfer cross section σ is roughly a constant, independent of ion drift velocity u; thus the diffusion coefficient D_a depends on u. Godyak[3] has solved for the density profile in this case and has extrapolated his solution to the low pressure limit[25] of collisionless ion flow in the bulk plasma, obtaining the expression

$$\cos\theta \approx \frac{0.86}{\left[3 + \dfrac{l_p}{2\lambda}\right]^{1/2}} \, ,$$

(20)

where $\lambda = (N\sigma)^{-1}$ is the mean free path, with N the neutral density. Using (20) and the definition of κ to eliminate θ from (18), and estimating[24] $\lambda \approx (300p)^{-1}$ cm, we obtain D_a as a function of p, l_p, and T_e. For high pressures, $\theta \approx \pi/2$ and we note that $D_a \propto p^{-1/2}$. For γ small, the use of (18) rather than (15) to determine D_a introduces negligible errors.

Sheath dynamics — The self-consistent solution for the dynamics of a capacitive r.f. sheath driven by a sinusoidal current source has been obtained by Godyak[3] and by Lieberman[26], under the conditions of time-independent collisionless ion motion and inertialess electron motion and by Lieberman[27] for collisional ion motion. The solutions account for both the nonuniform ion density and the time-average electron density within the sheath. The collisionless and collisional solutions have been joined heuristically to obtain the following three relationships:

First, the sheaths act as capacitors; in other words, there is a displacement current flow across each sheath, which can be written as

$$J_{rf} = K_{rf} \frac{\omega\varepsilon_0}{s_0} \frac{V_{rf}}{2} \, ,$$

(21)

where

$$K_{rf} = \frac{1.52(s_0/\lambda)^{1/2} + 1.23}{1 + (s_0/\lambda)^{1/2}}$$

(22)

encompasses both collisionless and collisional sheaths, ε_0 is the permittivity of free space, and V_{rf} is the r.m.s. r.f. voltage applied to the discharge.

Second, the d.c. ion current flow through the sheath has the form of Child's law,

$$J_i = K_i \varepsilon_0 \left[\frac{2e}{M} \right]^{1/2} \frac{V_s^{3/2}}{s_0^2} \ , \tag{23}$$

where

$$J_i = e n_0 u_B \cos\theta \tag{24}$$

is the d.c. ion current density to the electrodes and where

$$K_i = \frac{1}{1.22 + 0.48 \, (s_0/\lambda)^{1/2}} \tag{25}$$

encompasses collisionless and collisional sheaths.

Third, the peak values of the r.f. and d.c. voltages across each sheath must be comparable in order to confine the plasma electrons between the sheaths while allowing for some electrons to escape when the r.f. voltage reaches its peak value, so as to maintain quasineutrality within the discharge. For eV_{rf} large compared to kT_e, we can ignore the thermal corrections to obtain

$$V_s \approx 0.83 \, \frac{\sqrt{2}}{2} V_{rf} \ . \tag{26}$$

The factor 0.83 arises because the r.f. sheath voltage is a nonlinear function of the sinusoidal r.f. current density.

Electron energy balance — The power gained by the sheath and bulk electrons through ohmic heating and through stochastic heating by the oscillating sheath-plasma boundaries must be equal to the power lost by collisions to the neutrals and by escape from the plasma to the electrodes:

$$P_{el} = P_{sheath} + P_{bulk} + P_{stoc} = P_{coll} + P_{esc} \ . \tag{27}$$

The bulk ohmic power can be written as

$$P_{bulk} = 2 \int_0^{l/2} \frac{m\nu_m}{e^2 n(z)} J_{rf}^2 A \ dz \ ,$$

where ν_m is the electron-neutral momentum transfer frequency. The average of $1/n$ is weakly dependent on the detailed profile. For simplicity, we assume $\Lambda_{se} = 0$ when averaging. Evaluating the

integral, we obtain

$$P_{bulk} = \frac{m\nu_m}{e^2 n_0} \frac{1}{\theta} \ln[\tan(\theta/2 + \pi/4)](l - 2s_0)J_{rf}^2 A \ . \tag{28}$$

The ohmic heating in the sheath is evaluated in the Appendix using the expressions given in reference 26, yielding

$$P_{sheath} = \frac{m\nu_m}{e^2 n_0} \frac{1}{\cos\theta}[0.43H + 1.16 + 2.40/H]J_{rf}^2 s_0 A \ , \tag{29}$$

where $H = 0.60(V_s/T_e)^{1/2}$. For $V_s \gg T_e$ and significant sheath thicknesses, the ohmic heating in the sheaths can be comparable to or larger than the bulk ohmic heating.

The stochastic power is given by the expression[26-27]

$$P_{stoc} = [K_{stoc}(s_0/\lambda_D)^{2/3}]\frac{m}{e^2 n_0 \cos\theta} u_e J_{rf}^2 A \ , \tag{30}$$

where

$$K_{stoc} = \frac{1}{1.49 + 0.93(s_0/\lambda)^{1/3}} \tag{31}$$

encompasses both collisionless and collisional ion motion, λ_D is the Debye length at the plasma-sheath edge $z = s_0$, and $u_e = (8kT_e/\pi m)^{1/2}$ is the mean electron speed. The term to the right of the square brackets in (30) is the basic expression for the stochastic heating power obtained by Godyak[3], whereas the term within the brackets accounts for the nonuniform ion density and the time-varying electron density in the sheaths[26].

The energy $\mathcal{E}_c$ lost by thermal electrons per electron-ion pair created is due to ionization, excitation and elastic scattering against neutral gas atoms. The power lost through collisions by the electrons is then

$$P_{coll} = 2e\nu_{iz}\mathcal{E}_c \int_{s_0}^{1/2} n(z)A\ dz \ . $$

As previously, we let $\Lambda_{se} = 0$ to evaluate the integral, obtaining

$$P_{coll} = en_0 \nu_{iz} \mathcal{E}_c \frac{\sin\theta}{\theta} (l - 2s_0) A . \tag{32}$$

Although not fully self-consistent, the power carried away by the electrons escaping the plasma is

$$P_{esc} = 2e\Gamma\mathcal{E}_e A = 2en_0 \cos\theta\, u_B \mathcal{E}_e A , \tag{33}$$

where $\mathcal{E}_e \approx 4kT_e$ is the average energy of the escaping electrons. Using (28)-(30) and (32)-(33) in (27), we obtain the electron energy balance equation.

Total energy balance — The r.f. power is transferred to the charged particles in the discharge through the fields in the sheaths and in the plasma. Specifically, the r.f. supply provides power to the ions escaping the plasma $(2J_i V_s)$, the secondary electrons being injected into the plasma $(2\gamma J_i V_s)$, and the thermal electrons in the plasma [the term P_{el} in (27)]. Therefore, the total energy balance equation is

$$P_{rf} = 2J_i(1+\gamma)V_s + P_{el} . \tag{34}$$

III. RESULTS AND DISCUSSION

Given the control parameters p, l, V_{rf}, ω, and γ, a computer code DISCH has been developed[23] to solve the model equations to determine T_e, n_0, P_{rf}, J_i, J_{rf}, s_0, V_s, and the effective discharge circuit parameters. In order to obtain the solution, the ionization, excitation, elastic scattering, and momentum transfer collision frequencies (ν_{iz}, ν_{exc}, ν_{el}, and ν_m) and the energy $\mathcal{E}_c$ lost per electron-ion pair created are first determined by averaging over the assumed thermal electron energy distribution function $f(\mathcal{E})$. Letting $\nu = NR$ be the appropriate average collision frequency, where N is the neutral gas density and R is the collision reaction rate, then we obtain

$$R = \int_0^\infty d\mathcal{E} f(\mathcal{E}) (2\mathcal{E}/m)^{1/2} \sigma(\mathcal{E}) , \tag{35}$$

where σ is the experimental, energy-dependent cross section and the normalization $\int_0^\infty d\mathcal{E} f = 1$ has been assumed. If f is chosen to be a Maxwellian distribution, then (35) determines R as a function of T_e alone. The energy $\mathcal{E}_c$ lost per electron-ion pair created is given by

$$\mathcal{E}_c = \mathcal{E}_{iz} + 3\frac{m}{M}T_e\frac{R_{el}}{R_{iz}} + \mathcal{E}_{exc}\frac{R_{exc}}{R_{iz}} , \qquad\qquad (36)$$

where $\mathcal{E}_{iz}$ and $\mathcal{E}_{exc}$ are the energies lost per ionization and excitation collision, respectively. The momentum transfer frequency is given by $\nu_m = \nu_{el} + \nu_{iz} + \nu_{exc}$. Figure 2 shows the calculated reaction rates for a Maxwellian distribution of electrons in argon gas, and Fig. 3 shows the energy lost per electron-ion pair created in argon gas, using the cross section data presented in reference 24.

A typical discharge — The model has been applied to study the effect of different parameters on typical discharges. Figure 4 shows P_{rf}, T_e, and n_0 for a discharge in argon when the applied voltage is constant and the pressure p is varied between 1 and 100 mTorr, with the secondary emission coefficient γ as a parameter. Figure 4(a) shows that the power is relatively constant with pressure and that secondary electrons significantly increase the power at the higher pressures, where they are efficiently trapped near the electrodes and thus contribute to an increase in the density near the sheath edge. The electron temperature shown in Fig. 4(b) follows the trend measured in d.c. discharges. Secondary electrons affect the bulk temperature only weakly; T_e falls slightly as γ increases because the bulk electrons play less of a role in producing the ionization required to maintain the discharge. Figure 4(c) displays the behavior of the central electron density and shows that it increases roughly linearly with pressure. This results from an increasing θ. The edge density remains fairly constant with p, which is consistent with the small variation of power with p.

Model assumptions — The model equations have been used to compare the effects of different physical processes incorporated into the basic equations. Figure 5 shows P_{rf}, T_e, and n_0 versus p for a set of four "gedanken" models as follows:

1. No secondary electrons ($\gamma = 0$), uniform ion density [(19) is used in place of (15)], and no stochastic heating ($P_{stoc} = 0$).

2. No secondary electrons ($\gamma = 0$), nonuniform ion density [(18) is used instead of (15)], and $P_{stoc} = 0$.

3. Same as 2 with secondary electrons [$\gamma = 0.1$, (15) is used, $P_{stoc} = 0$].

4. Same as 3 with stochastic heating [P_{stoc} given by (30)].

We can see how the effects of secondary electrons at high pressures and of stochastic heating at low pressures change the results predicted by model 2. Specifically, secondary electrons slightly increase the power absorbed by the discharge at high pressures due to the increase in the density near the sheath edge that they generate. The main effect is stochastic heating, which dramatically increases the absorbed power and the peak density at low pressures. Without stochastic heating, the plasma will not sustain itself at the lowest pressures (discontinuity on the graphs).

Comparison with experiments — Figure 6 compares the r.f. power absorbed in an argon discharge with measurements published by Logan et al[28]. The model predicts the variation of P_{rf} versus V_{rf} at a fixed pressure quite well, although the experimentally measured value of P_{rf} is a factor of approximately four larger than that predicted by the model. The r.f. power applied to an argon discharge has also been measured in our laboratory and compared to the results predicted by the model. Figure 7 shows measurements of P_{rf} versus p for two different values of the applied voltage V_{rf}. The secondary electron emission coefficient was arbitrarily chosen to be 0.1. Again, the variations of P_{rf} with p are in reasonable agreement with the model, but the absolute value of the model predictions are a factor of approximately four lower than the experimental measurements.

The results indicate that, at least at the lower pressures, the dominant heating is from electron collisions with the oscillating sheath. At the lower pressures, secondaries are lost rapidly and therefore contribute little to the overall dynamics.

The factor of four discrepancy between the predicted and measured absorbed power has not been explained. A contributing cause is probably the asymmetry of the experimental discharges. We know that asymmetry exists in our experiment because a d.c. bias voltage comparable to the applied r.f. voltage is measured on the powered electrode. Models for asymmetric discharges similar to the one presented here are currently under development[29]. Another factor that could increase the power is higher secondary emission coefficients. Our assumed γ's are probably on the low side[30]. There is also some reason to believe that the power measurement overestimates the power actually delivered to the plasma[31]. Both better power and density measurements will be needed as the theory is extended to

model the experimental configuration more closely.

APPENDIX

The ohmic heating in the sheaths can be found from the results presented in reference 26. For a sinusoidal r.f. current density $\sqrt{2}J_{rf}\sin\omega t$, the instantaneous ohmic power per unit area dissipated in one sheath is

$$S(t) = \int_0^s \frac{2m\nu_m}{e^2 n(s)} J_{rf}^2 \sin^2\omega t \, ds \, , \tag{A1}$$

where $s(\phi)$ is the instantaneous position of the oscillating electron sheath edge at the phase $\phi = \omega t$. Writing $ds/n(s) = (ds/d\phi)d\phi/n(\phi)$ and using equations (18) and (23) in reference 26 to determine $ds/d\phi$ and $n(\phi)$, we obtain

$$S(t) = \frac{2m\nu_m}{e^2 n_0 \cos\theta} J_{rf}^2 s_0 \sin^2\omega t \int_0^{\omega t} d\phi \sin\phi A^2(\phi) \, , \tag{A2}$$

where

$$A(\phi) = 1 - H\left[\frac{3}{8}\sin 2\phi - \frac{1}{4}\phi\cos 2\phi - \frac{1}{2}\phi\right] \, ,$$

$s_0 = \sqrt{2}J_{rf}/(e\omega n_0 \cos\theta)$, and $H = s_0^2/(\pi\lambda_D^2)$ [see equations (19) and (21) in reference 26]. Averaging (A2) over the phase interval $\omega t = (0, \pi)$, reversing the order of the ϕ and ωt integrations, and integrating with respect to ωt, we obtain

$$\overline{S} = \frac{2m\nu_m J_{rf}^2}{e^2 n_0 \cos\theta} \frac{s_0}{\pi} \int_0^\pi d\phi \sin\phi A^2(\phi) \left[\frac{1}{4}\sin 2\phi - \frac{1}{2}\phi + \frac{1}{2}\pi\right] \, . \tag{A3}$$

Integrating (A3) with respect to ϕ and writing $P_{sheath} = 2\overline{S}A$, we obtain (29).

REFERENCES

1. J.H. Keller and W.P. Pennebaker, *IBM J. Res. and Develop.* 23, 3 (1979).

2. J.A. Taillet, *J. Physique-Lettres* 40, 223 (1979).

3. V.A. Godyak, *Soviet Radio Frequency Discharge Research,* Technical Report, Delphic Associates Inc., Falls Church, VA (1986).

4. V.A. Godyak and A.S. Kanneh, *IEEE Trans. Plasma Sci.* PS-14, 112 (1986).

5. O.A. Popov and V.A. Godyak, *J. Appl. Phys.* 57, 53 (1985).

6. V.A. Godyak and A. Kh. Ganna, *Sov. J. Plasma Phys.* 6, 372 (1980).

7. V.A. Godyak and A. Kh. Ganna, *Sov. J. Plasma Phys.* 5, 376 (1979).

8. V.A. Godyak and O.A. Popov, *Sov. J. Plasma Phys.* 5, 227 (1979).

9. V.A. Godyak, *Sov. J. Plasma Phys.* 2, 78 (1976).

10. B. Chapman, *Glow Discharge Processes,* John Wiley & Sons, New York, NY (1980).

11. J.W. Coburn and H.F. Winters, *J. Vac. Sci. Technol.* 16, 391 (1979).

12. J.H. Keller, K. Kohler, J.W. Coburn, D.E. Horne, and E. Kay, *J. Appl. Phys.* 57, 59 (1985).

13. A.D. Richards and H.H. Sawin, *J. Appl. Phys.* 62, 799 (1987).

14. M.J. Kushner, *J. Appl. Phys.* 54, 4958 (1983).

15. M.J. Kushner, *IEEE Trans. Plasma Sci.* PS-14, 188 (1986).

16. W.S. Lawson, M.A. Lieberman, and C.K. Birdsall, "Electron Dynamics of RF Driven Parallel Plate Reactor", Abstract 3P5, Fifteenth IEEE International Conference on Plasma Science, Seattle, WA, June 6-8, 1988.

17. R.W. Boswell and I.J. Morey, *Appl. Phys. Lett.* 52, 21 (1988).

18. D.B. Graves, *J. Appl. Phys.* 62, 88 (1987).

19. D.B. Graves and K.F. Jensen, *IEEE Trans. Plasma Sci.* PS-14, 78 (1986).

20. J.P. Boeuf, "Modeling of R.F. Glow Discharges", Abstract M-1, 41st Annual Gaseous Electronics Conference, Minneapolis, MN, Oct. 18-21, 1988.

21. E. Gogolides, J.P. Nicolai and H.H. Sawin, "Continuum Modeling of SF_6 and Ar R.F. Discharges, and Comparison with Experimental Measurements,", Abstract M-2, 41st Annual Gaseous Electronics Conference, Minneapolis, MN, Oct. 18-21, 1988.

22. A.P. Paranjpe, J.P. McVittie and S.A. Self, "Numerical Simulation of 13.56 MHz Symmetric Parallel Plate R.F. Glow Discharges in Argon," Abstract E-5, 41st Annual Gaseous Electronics Conference, Minneapolis, MN, Oct. 18-21, 1988.

23. G.R. Misium, "Modeling of RF Plasma Discharges for IC Processing", M.Eng. Thesis, College of Engineering, University of California, Berkeley, CA (1988).

24. E.A. McDaniel, *Collision Phenomena in Ionized Gases*, John Wiley & Sons, New York, NY (1964).

25. L. Tonks and I. Langmuir, *Phys. Rev.* **34**, 876 (1929).

26. M.A. Lieberman, *IEEE Trans. Plasma Sci.* **16**, 638 (1988).

27. M.A. Lieberman, "Dynamics of a Collisional Capacitive R.F. Sheath," Memo UCB/ERL M88/62, Electronics Research Laboratory, College of Engineering, University of California, Berkeley (1988); to appear in *IEEE Transactions on Plasma Science* (1989).

28. J.S. Logan, N.M. Mazza and P.D. Davidse, *J. Vac. Sci. Technol.* **6**, 120 (1969).

29. M.A. Lieberman and S.E. Savas, "Ion Diffusion and Electrode Bias Voltage in Asymmetric Capacitive R.F. Discharges, Abstract H-4, 41st Annual Gaseous Electronics Conference, Minneapolis, MN, Oct. 18-21, 1988; see also M.A. Lieberman, "Spherical Shell Model of an Asymmetric R.F. Discharge," Memo UCB/ERL M88/65, Electronics Research Laboratory, College of Engineering, University of California, Berkeley (1988); submitted to *Journal of Applied Physics*.

30. B. Szapiro, J.J. Rocca and Prabhuram T., "Electron Yield of Glow Discharge Cathode Materials under Noble Gas Ion Bombardment," Abstract GB-3, 41st Annual Gaseous Electronics Conference, Minneapolis, MN, Oct. 18-21, 1988.

31. W.G.M. van den Hoek, C.A.M. de Vries, and M.G.J. Heijman, *J. Vac. Sci. Technol.* **B5**, 647 (1987).
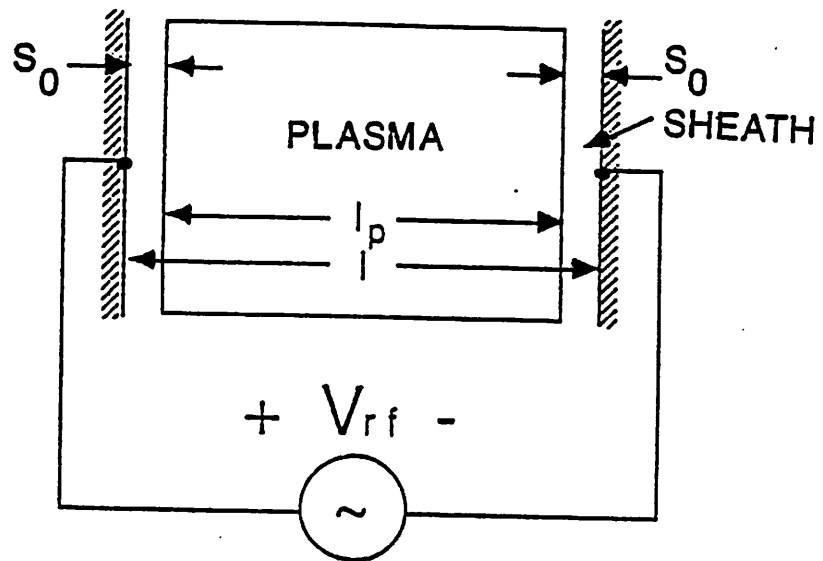
Fig. 1.   Geometry of a symmetric, capacitive r.f. discharge.

Fig. 2. Electron-collision rate coefficients in argon gas.
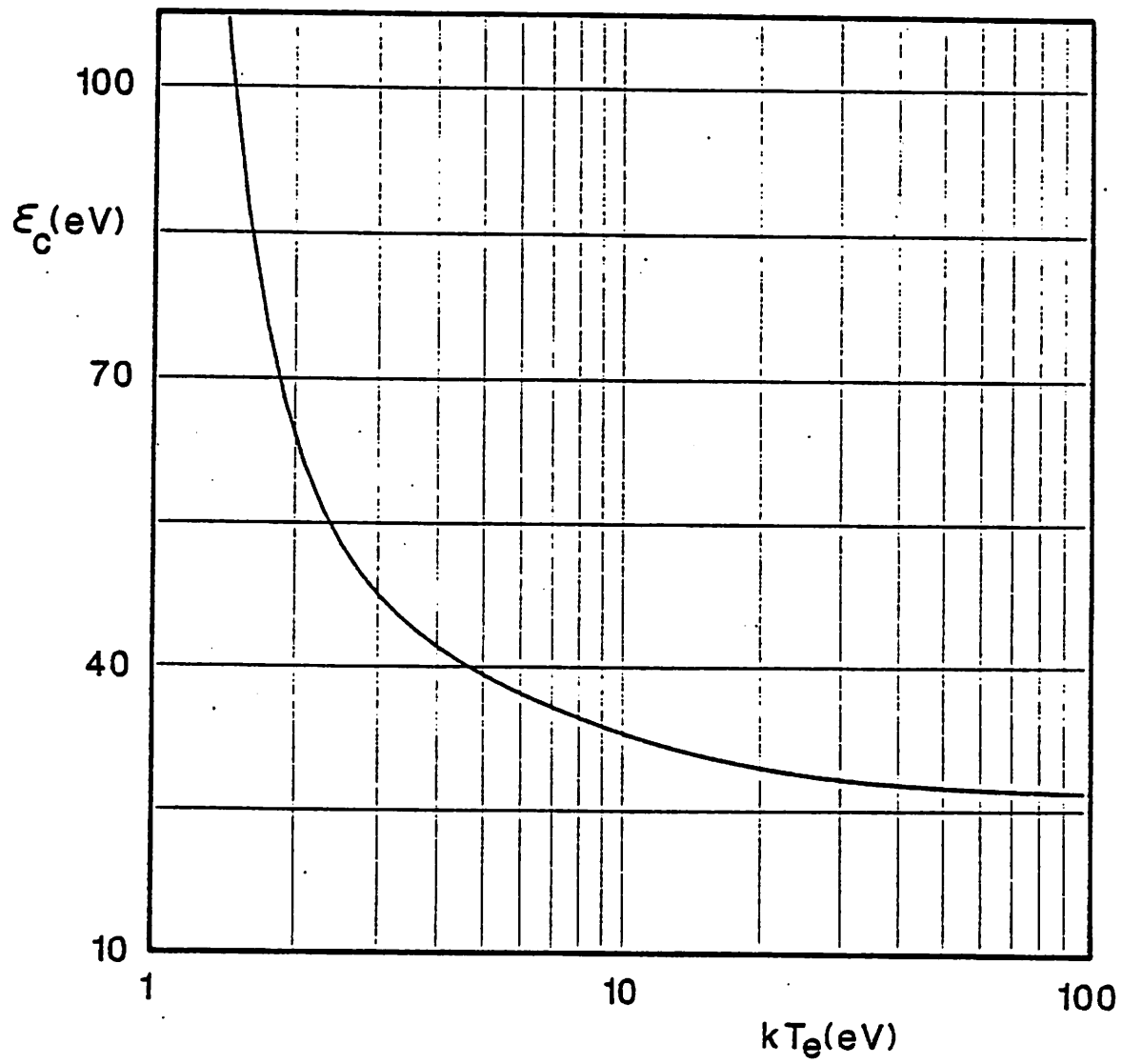
Fig. 3. Electron energy loss $\mathcal{E}_c$ per electron-ion pair created.

Fig. 4. Results for a typical symmetric parallel plate discharge in argon: frequency 13.56 MHz, V_{rf} = 330 V, A = 410 cm^2, l = 3 cm; (a) r.f. power; (b) electron temperature; (c) peak electron density.
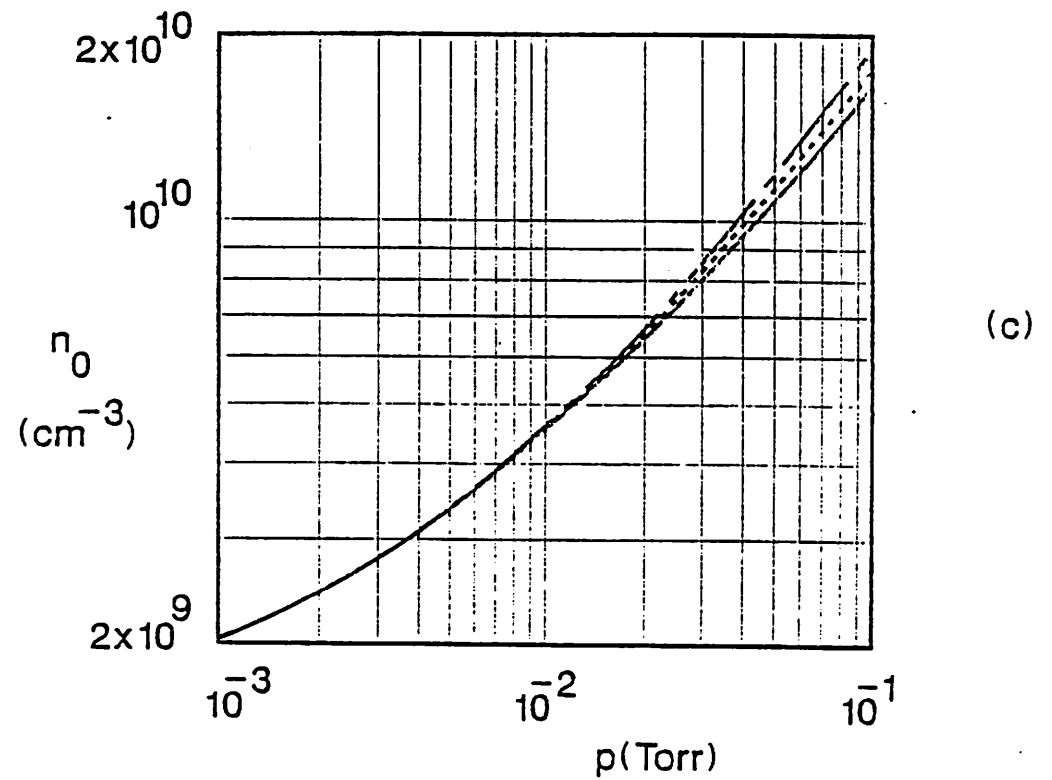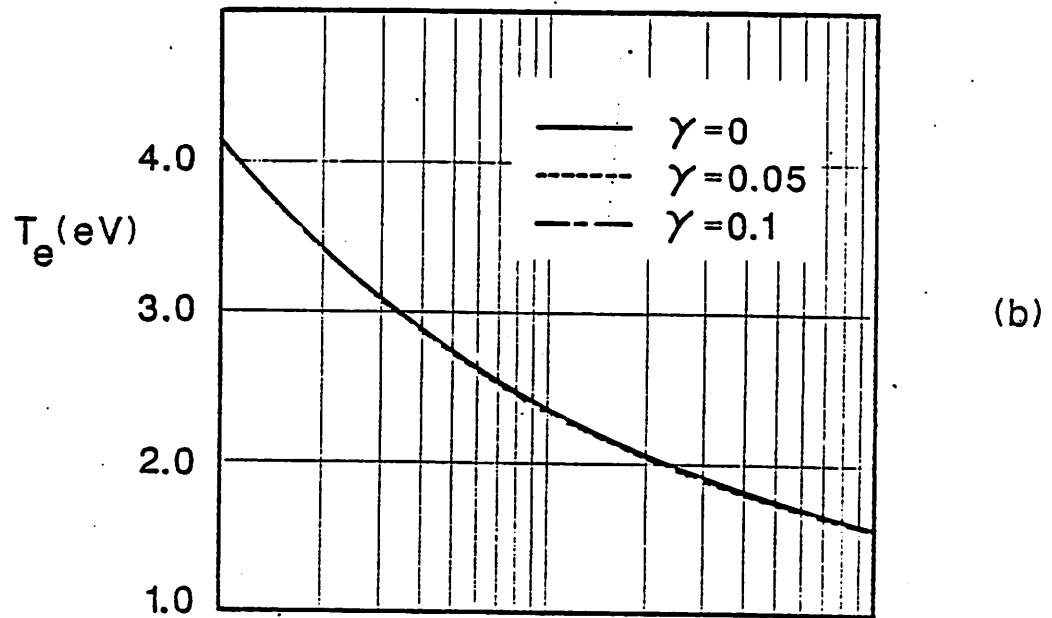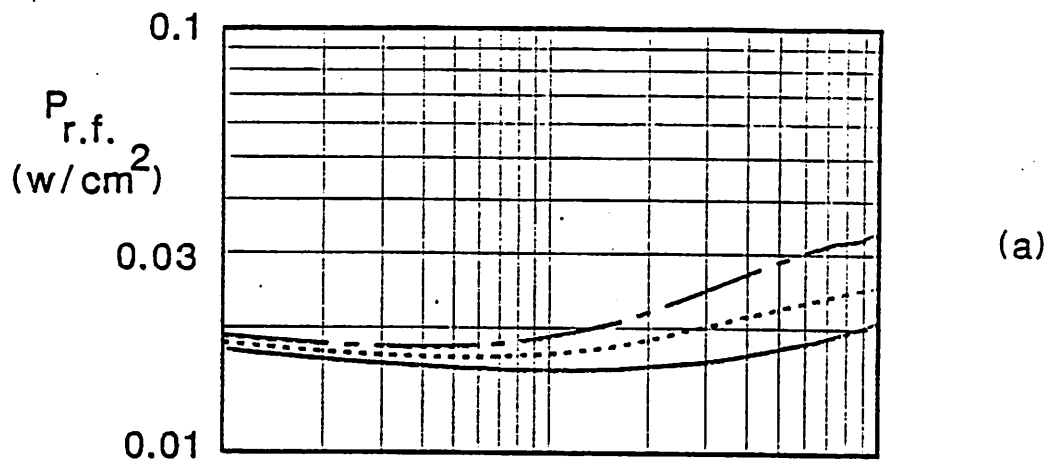
Fig. 5. Results for four different model assumptions for a symmetric discharge in argon: frequency 13.56 MHz, $V_{rf} = 250$ V, $A = 410$ cm^2, $l = 10$ cm, $\gamma = 0.1$; (a) r.f. power; (b) electron temperature; (c) peak electron density.
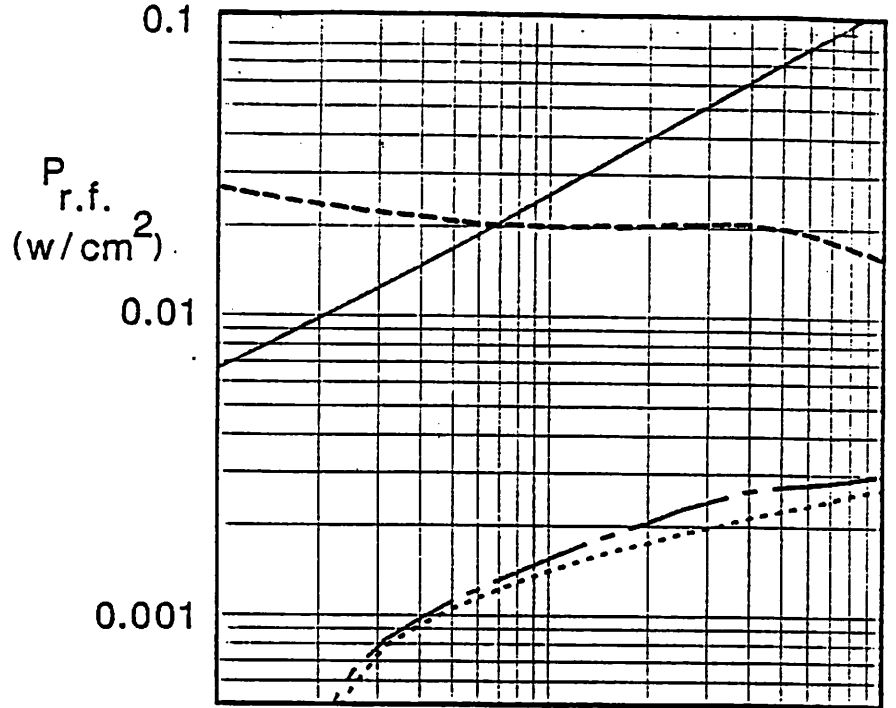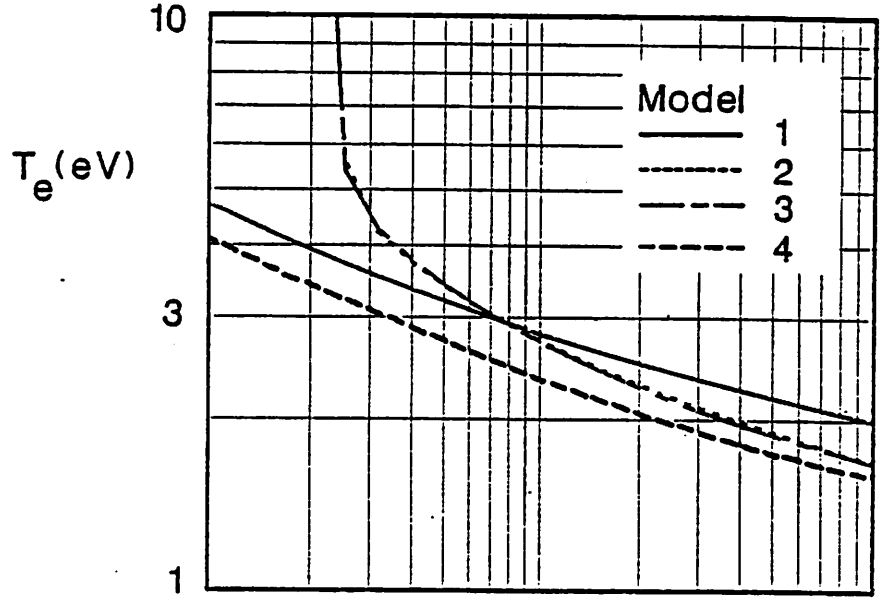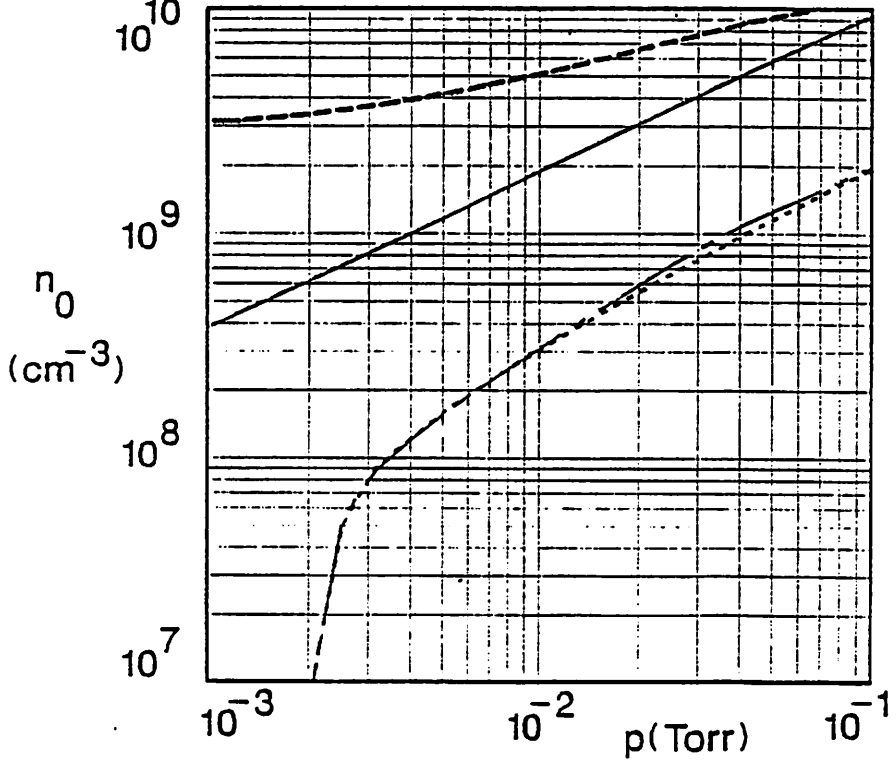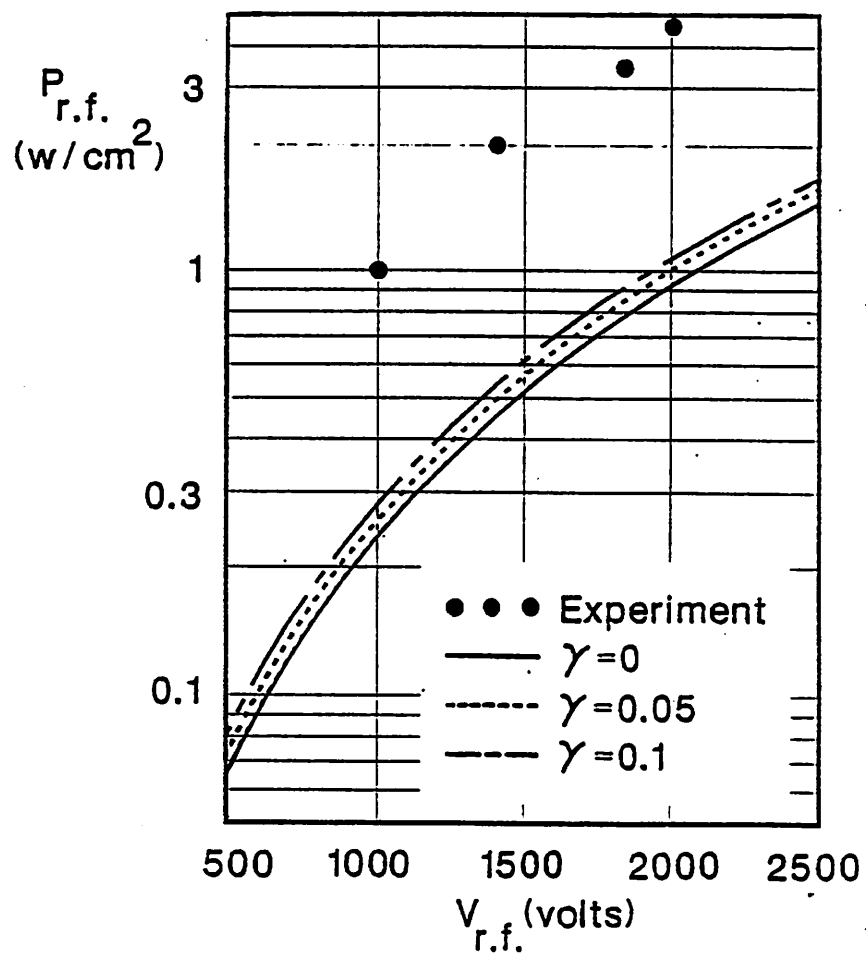
Fig. 6. R.f. power versus voltage in an experimental discharge.
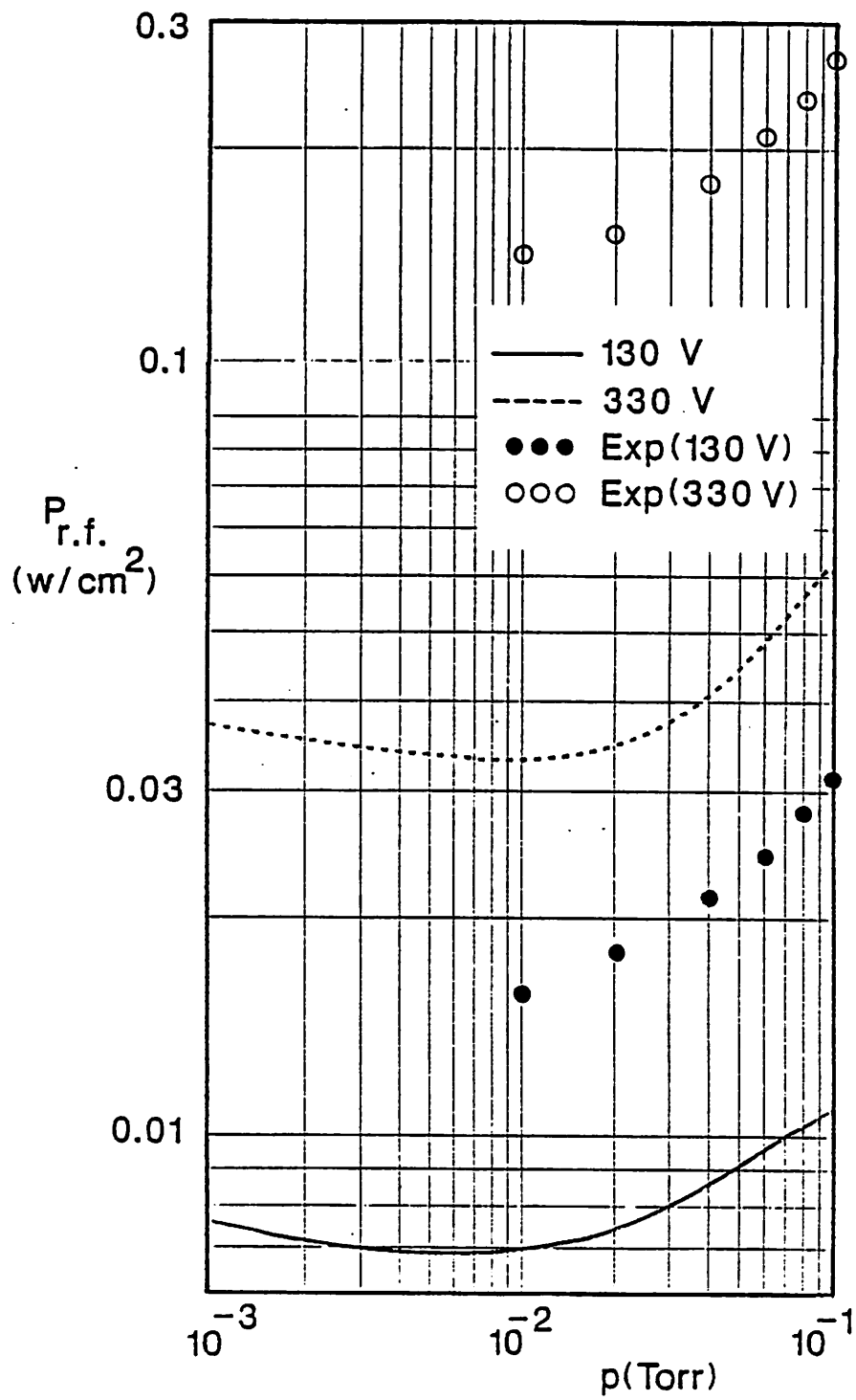
Fig. 7.   R.f. power versus pressure in an experimental discharge for two applied voltages.